

Supplementary Information for the manuscript “Electronic properties of germanane field effect transistors”

Table of contents

X-ray diffraction	1
FTIR spectroscopy	5
UV-Vis-NIR/DRA measurements	5
Raman spectroscopy	6
Resistance model for 4-terminal measurements	7
Non-linear I-V characteristics	7
Four-terminal transfer curves at higher gate voltage range	8
Electrical characterization of sample #2	9

X-ray diffraction

Single-crystal X-ray diffraction (XRD) measurements were performed using a Bruker D8 Venture diffractometer operating with Mo $K\alpha$ radiation and equipped with a Triumph monochromator and a Photon100 area detector. The crystals were mounted on a 0.3 mm nylon loop using cryo-oil. An Oxford Cryosystems Cryostream Plus was used to cool the samples to 100 K for data collection using a nitrogen flow. Data processing was performed using the Bruker Apex II software; the structure was solved by direct methods and refined using the SHELXL software [1]. Powder XRD data were collected using a Bruker D8 Advance diffractometer operating in Bragg-Brentano geometry with Cu $K\alpha$ radiation. The data were fitted using the GSAS software suite [2].

The sample contained many small, dark brown crystals. A rectangular block-like crystal of dimensions $0.1 \times 0.05 \times 0.02$ mm was chosen for structure determination by single-crystal XRD. The unit cell was found to be monoclinic with lattice parameters $a = 6.9244(14)$ Å, $b = 3.9978(14)$ Å, $c = 10.939(5)$ Å, $\beta = 102.181(1)^\circ$. Inspection of reconstructed reciprocal lattice sections (Fig. S1) showed that the condition $h+k=2n$ is obeyed, implying a C-centered lattice. Intensity statistics suggested a non-centrosymmetric structure, thus structure solution and refinement were attempted in space groups C2 and Cm. The Ge framework structure was solved by direct methods using the intensities of 373 unique reflections and the best solution (in terms of goodness of fit and residual electron density) was obtained using C2. Hydrogen atoms were added using the “riding” model incorporated in SHELXL, assuming tetrahedral

coordination of Ge and fixed Ge-H bond distances of 1.565 Å [4]. A view of the refined structure is shown in Fig. S2 and the atomic parameters are listed in Table S1.

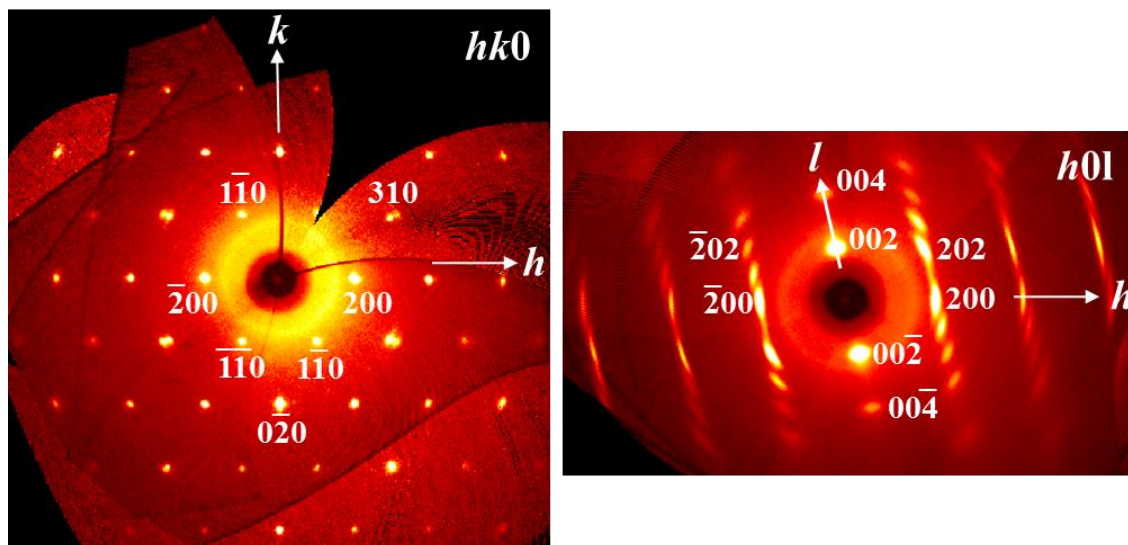


Figure S1: *hk0* and *h0l* reciprocal lattice images reconstructed from raw single-crystal XRD data.

Table S1: Refined atomic coordinates and displacement factors for germanane at 100 K. Hydrogen positions were generated automatically by geometrical considerations.

Space group *C2*: $a = 6.9244(14)$ Å, $b = 3.9978(14)$ Å, $c = 10.939(5)$ Å, $\beta = 102.181(1)^\circ$.

Atom	<i>x</i>	<i>y</i>	<i>z</i>	U_{11} (Å ²)	U_{22} (Å ²)	U_{33} (Å ²)	U_{12} (Å ²)	U_{13} (Å ²)	U_{23} (Å ²)
Ge1	0.6557(8)	0.3589(16)	0.9678(9)	0.012(3)	0.029(4)	0.131(8)	-0.001(4)	0.029(3)	0.005(4)
Ge2	0.6784(18)	0.9306(16)	0.5386(14)	0.092(8)	0.018(4)	0.202(13)	0.005(4)	0.041(8)	-0.003(4)
H1	0.6069	0.3589	0.8214	0.067					
H2	0.7267	0.9306	0.6850	0.123					

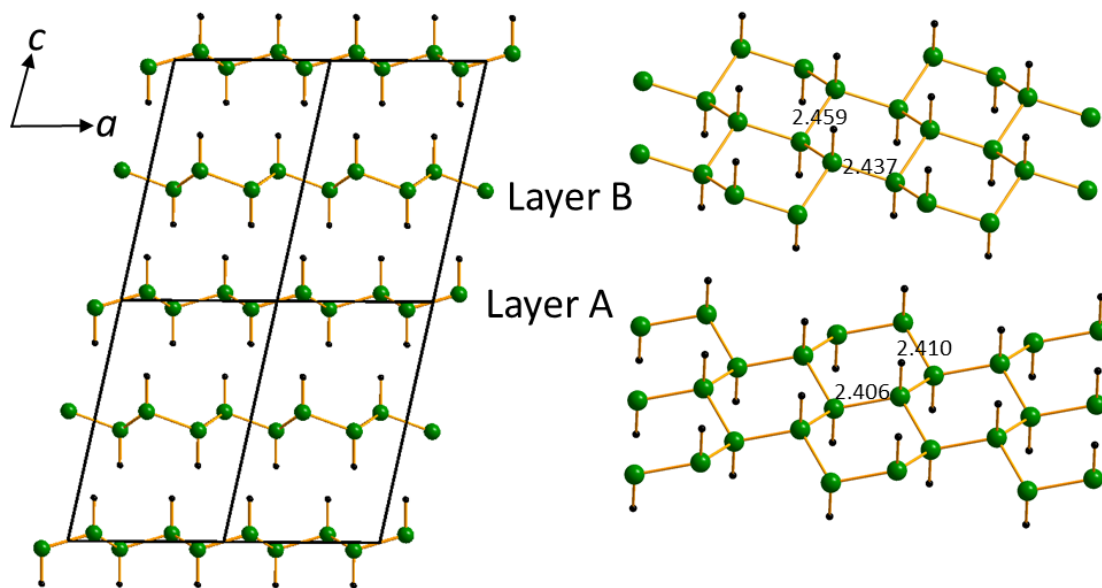


Figure S2: Refined crystal structure from single-crystal XRD data. The 6-membered Ge rings adopt the “chair” configuration. Views of layers A and B (right) show the crystallographically distinct Ge-Ge bond distances (Ångstrom).

In Fig. S1 it is apparent that the pseudo-hexagonal $hk0$ -plane (left) is well defined, containing sharp spots, whereas the spots along the l -direction (right) exhibit streaking, indicating short range order in the layer stacking direction. This is consistent with a previous report on germanane [3]. Nevertheless, the $00l$ spots are well distinguished, allowing the average stacking periodicity to be established.

In the refined structure in Fig. S2 it can be seen that the Ge atoms form 6-membered rings in the “chair” configuration. There are two crystallographically independent layers which are stacked in an ABAB sequence along the c -axis. The lateral offset between successive layers gives rise to a monoclinic unit cell. The seventh layer is almost directly above the first layer; this would correspond to the 6-layer rhombohedral unit cell of β -CaGe₂ (space group R-3m) with which Luo and Zurek [4] argued that germanane should be isostructural. The transformation from the rhombohedral to monoclinic cell is given by the matrix [1, -1, 0; 1, 1, 0; -1/3, 1/3, 1/3]. Indeed, our single-crystal XRD data could be indexed assuming a rhombohedral cell with $a = 3.998$ Å, $c = 32.078$ Å. We thus carried out structure solutions and refinements in the space groups R-3m, R3m and R3. The best fit was obtained in R3m but with an RF^2 factor slightly larger than the C2 solution (0.187 versus 0.177) and with a significantly larger residual electron density. We therefore conclude that the structure is very close to that of β -CaGe₂, but with a slight monoclinic distortion. We note that the RF^2 fit factors are relatively high due to the diffuse scattering associated with stacking disorder (Fig. S1).

The disorder in the stacking direction can also be seen in powder XRD patterns collected at room temperature and above on part of the bulk sample that was finely ground (Fig. S3). The intense 002 peak is extremely broad. The width of this peak

allows a rough estimate of the correlation length; use of the Scherrer formula gives an estimate of ~ 50 Å (~ 5 unit cells) in the c -direction. The strongly anisotropic peak broadening gives rise to problems in fitting the powder XRD pattern well, but the fit is rather good assuming the C2 structure obtained from the single crystal XRD data. There is a small amount of α -Ge in the sample: the ratio of GeH to α -Ge is 94(2)% to 6(2)%.

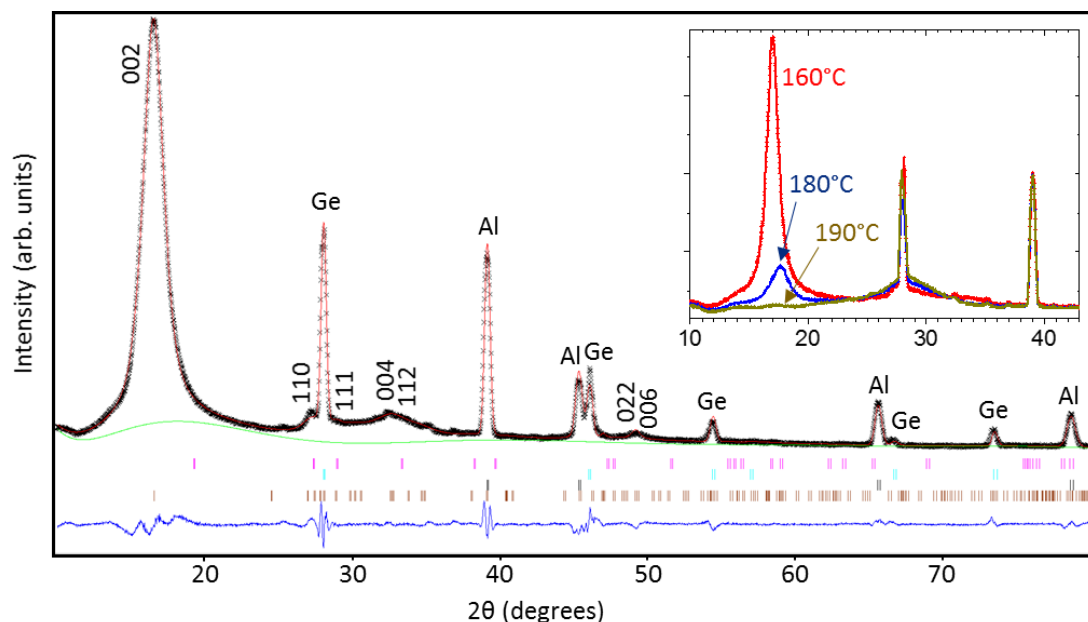


Figure S3: Observed (black data points), calculated (red line) and difference (blue line) powder XRD profiles at 40 °C. The Al peaks are from the sample holder. The inset shows the disappearance of the 002 peak as the sample is heated from 160 °C to 190 °C.

On heating, no changes are observed in the powder XRD patterns up to 160 °C apart from slight peak shifts due to thermal expansion. The GeH peaks decrease strongly in intensity at 180 °C and have disappeared at 190 °C (inset to Fig. S3). On cooling again the peaks do not reappear, implying that there is an irreversible crystalline to amorphous transition on heating.

~~Therefore, with XRD spectroscopy we unambiguously determine the crystallographic structure of the synthesised material to be identical to that of GeH₂~~

FTIR spectroscopy

Fourier transform infrared spectra were measured in the range of 400–4000 cm^{-1} with a Shimadzu FTIR 8400 spectrometer equipped with a deuterated triglycine sulfate (DTGS) detector. Each spectrum was the average of 32 scans collected with 2 cm^{-1} resolution. Samples were in the form of KBr pellets containing *ca.* 2 wt % of sample. The spectrum of germanane shows a strong peak at 2000 cm^{-1} due to Ge-H stretching vibration while peaks at 470, 574 and 620 cm^{-1} assigned to multiple wagging modes of Ge-H [3, 5]. Moreover, weak peaks at 760 and 825 cm^{-1} are also present which correspond to H-Ge-H bending modes from neighboring Ge atoms at the edges of the crystalline germanane layer and/or Ge vacancies within the layered germanane lattice [3].

Based on the above FTIR spectroscopy we confirmed hydrogen termination of germanium atoms in the synthesised germanane (GeH).

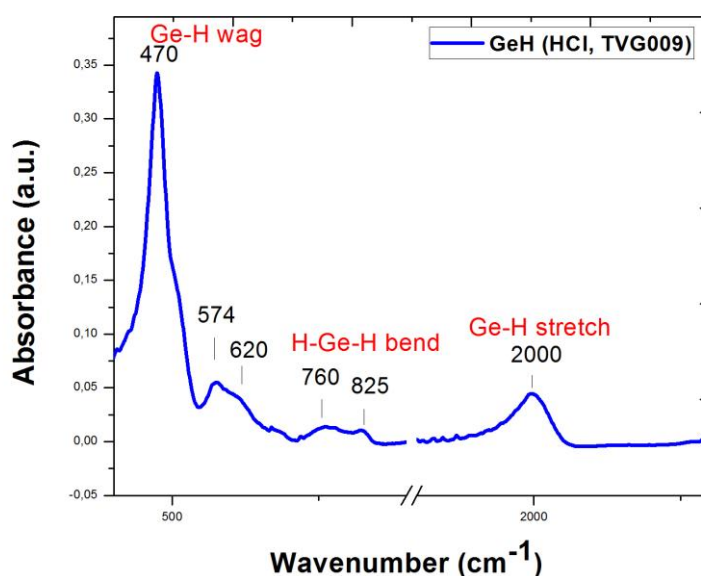


Figure S4. FTIR spectrum of GeH

UV-Vis-NIR/DRA measurements

The diffuse reflectance measurements were conducted using a Shimadzu UV-VIS-NIR Spectrophotometer (UV-3600) equipped with an integrating sphere attachment on barium sulfate coatings. The diffuse reflectance spectrum was converted to Kubelka-Munk function, $F(R_\infty)$ [3,6] and plotted against wavenumbers (nm) and photon energy (eV). The line tangent to the point of inflection on the curve and the eV value, at the point of intersection of the tangent line determined E_g value close to 1.58

eV. Thus, with DRA spectroscopy we confirm the presence of a band gap with the value which is very similar to that reported for germanane in Ref. [3].

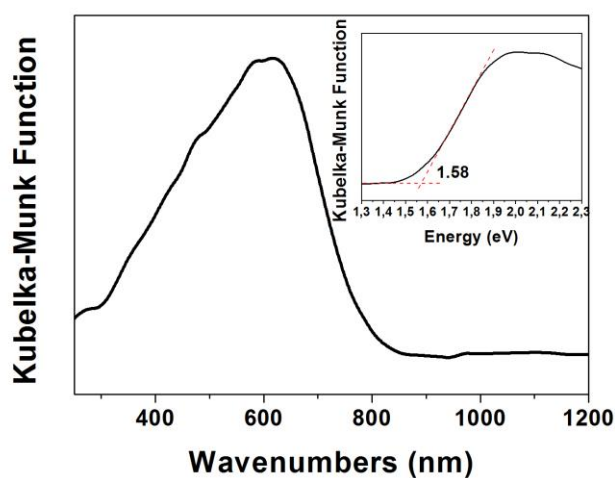


Figure S5. DRA spectrum of GeH plotted in Kubelka-Munk function versus wavenumbers/ photon energy

Raman spectroscopy

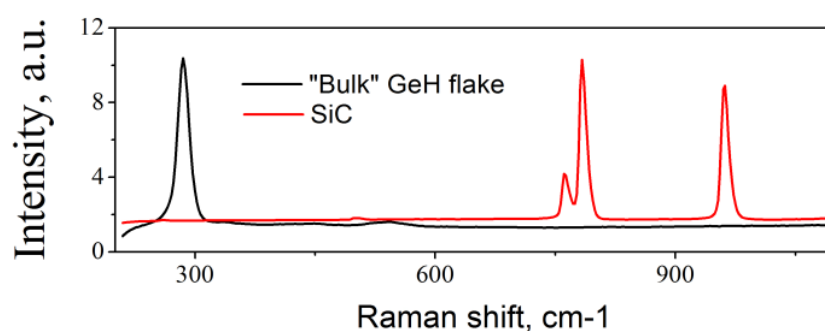


Figure S6. Raman spectrum of bulk germanane powder flake (black) transferred on top of a SiC substrate, where SiC spectrum (red) shown separately. A characteristic peak associated with Ge-H bond is seen at 285 cm⁻¹.

Raman spectra were collected using a 632.8 nm excitation laser with a spot size of 2 μm using an Olympus BX51 microscope coupled to a HeNe Laser (10 mW, Thorlabs) and a Shamrock 163 spectrograph and iDus-420-OE CCD (Andor Technology). The Raman spectrum of the synthesized powder flake clearly reveals the presence of the Ge-H bond in the studied material thus confirming its composition.

Resistance model for 4-terminal measurement

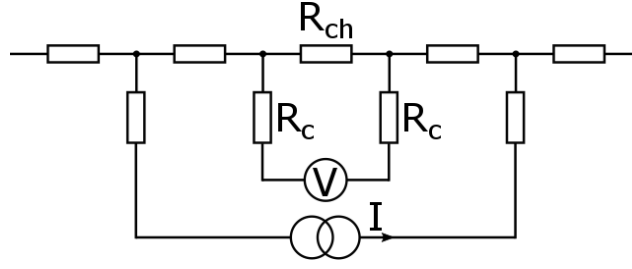


Figure S7. Schematics of the used resistance network model for multiterminal measurements. Horizontal resistances R_{ch} line represent the channel divided into sections between the contacts which are shown with vertical resistances R_c .

For interpretation of the 3- and 4-terminal measurements we employ a standard resistance network model shown in Fig. S7. Within such a model the contact contribution R_c is fully excluded when 4-terminal configurations is used. 3-terminal measurement unambiguously gives the contact resistance R_c . However, in reality the metal contact locally modifies the semiconductor channel underneath it, forming, for example, p-n junctions in the channel or depletion regions. This implies that $R_{ch} = r_{ch} + r_{ch}^*$, where r_{ch} is true unaffected channel resistance and r_{ch}^* is the part of the channel modified due to the contact. Under these circumstances even a 4-terminal configuration contains not only the intrinsic channel resistance but also contact induced contribution.

Non-linear I-V characteristics

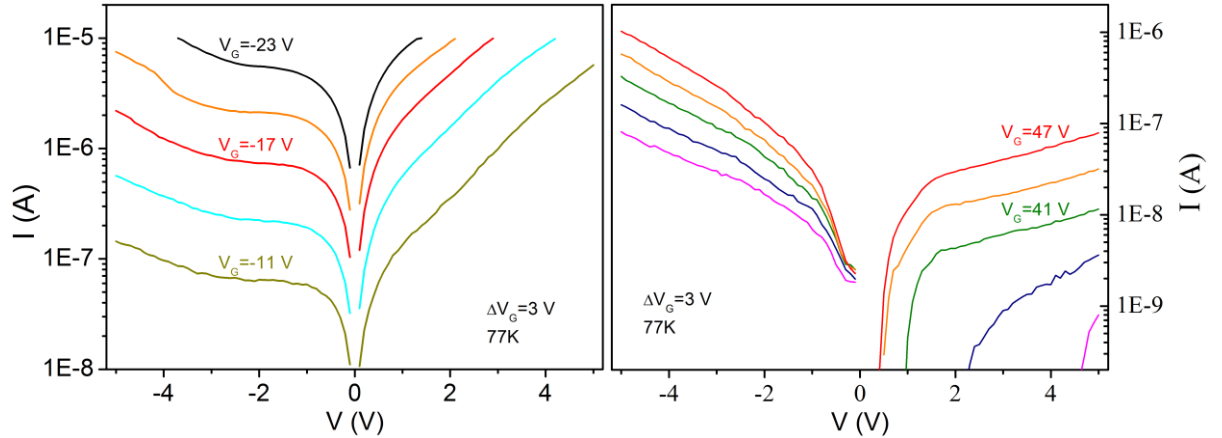


Figure S8. 2-terminal I-V characteristics of the device measured between contacts 18 and 19 and plotted in logarithmic scale with respect to the source-drain bias for different gate voltages for both hole doped (**left**) and electron doped (**right**) regimes. For $V < 0$ V the value of the current is multiplied with -1 for the applicability of the logarithmic scale.

We measured I-V characteristics of the device in 2-terminal configuration for different gate voltages, Fig S8. Overall the measured output curves resemble transistor-like behaviour. In particular, for $V < 0$ in a certain ranges of the gate voltage

we observed consistently a current saturation regime that is followed by a breakdown regime where the source-drain current transits into an exponential increase. However, at $V > 0$ a saturation regime is practically absent implying that the output curves are highly asymmetric with respect to $V = 0$. Assuming a homogeneous channel the strong asymmetry in I-V characteristics unambiguously suggests formation of nonequivalent Schottky barriers formed at source and drain contacts. This is not immediately expected as both of the contacts used for measurements are geometrically designed to be the same (contact 18 and 19 in Fig. 1, main text) and there is no step in our fabrication procedure that would make a clear distinction between them. Nevertheless, experimentally the 3-terminal dependences $V(V_G)$ for these contacts indeed reveal substantial difference in their resistances as seen in Fig. 2a, main text. With a certain extension this situation is similar to a p^+np bipolar transistor with similar asymmetric I-V characteristics.

Four-terminal transfer curves at higher gate voltage range

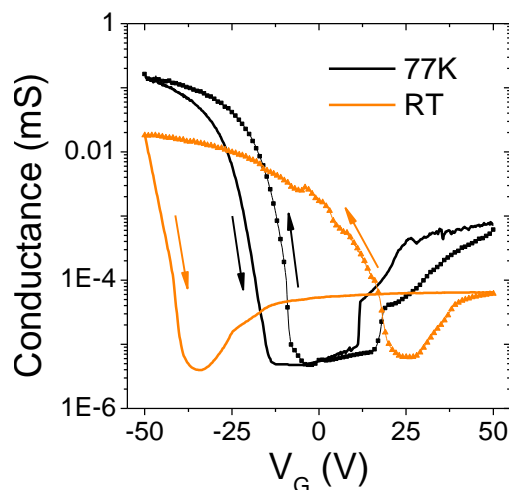


Figure S9. 4-terminal conductance plotted in a semilogarithmic scale as function of V_G for both room temperature (orange) and 77K (black). The current was applied between contacts 17 and 8, while the voltage was measured between contacts 19 and 13. Arrows indicate the direction of the sweeping gate voltage.

Higher gate voltages up to $\pm 50V$ (at 0.1 V/s sweep rate) were probed to achieve higher charge carrier concentration. In Fig. S9 conductance is plotted within a maximum used gate voltage range in semilogarithmic scale both at room temperature and 77K. The observed modulation of the conductance with applied V_G gives an on/off current ratio $\sim 10^4$ at room temperature and $\sim 10^5$ at 77K. As mentioned in the main text a significant hysteresis develops when V_G is swept in a range larger than $\pm 10V$. For a given range of $\pm 50V$ the difference in conductance minima positions in opposite sweeping directions is found to be as large as $\sim 60V$ at room temperature. Presence of such hysteresis is likely to be due to the existence of charge trap states.

Electrical characterization of sample #2

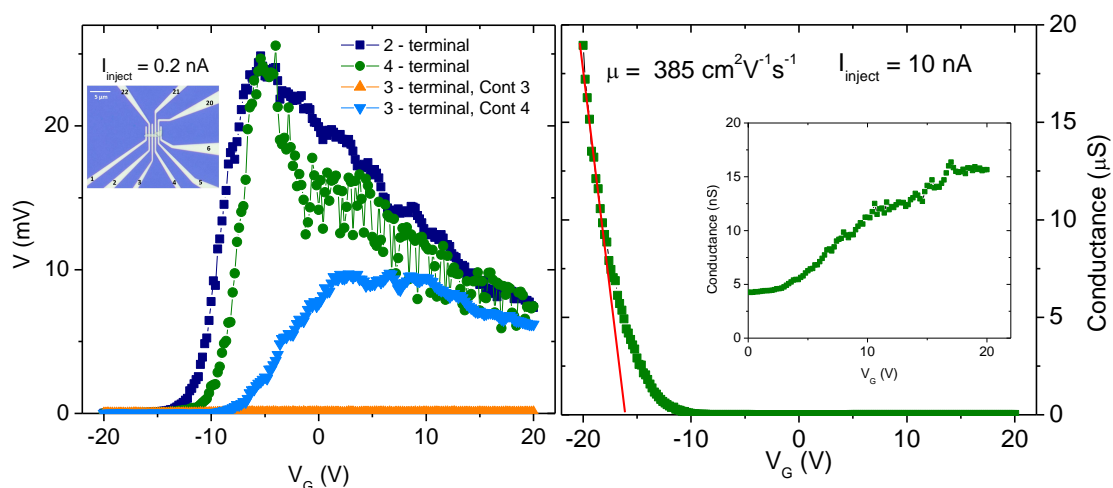


Figure S10. **Left:** measured signal V for sample #2 is plotted for 2-terminal (blue), 3-terminal (red) and 4-terminal (black) configurations as a function of the gate voltage. 3-terminal measurements are done for contacts 3 and 4. The applied constant current between source and drain is 0.2 nA, measurements are done at room temperature. inset - optical image of the device of germanane on SiO_2 substrate with Ti/Au electrodes. **Right:** 4-terminal conductivity V/I measured at room temperature as function of V_G . The red line represents a linear fit and gives $\sim 400 \text{ cm}^2/(\text{V}\cdot\text{s})$ for the hole mobility. The gate voltage is swept from negative to positive values. The inset shows a zoomed in region for positive gate voltage range of the dependence from the main panel.

One of the consequences of the formed Schottky barrier at the interface is a doped (depleted) region in the vicinity of the contact. The affected region spreads out as far as the depletion width (both in plane of the flake and beneath the contact) and can generally contribute to the electrical transport as an extra resistance. Depending on the thickness of the studied semiconductor with respect to the depletion width such regions/junctions will affect the 4-terminal measurements to a different extent. As compared to sample #1 discussed in the main text (see Figs. 2b,3) it is seen that contact contribution for sample #2 is much more pronounced even in a 4-terminal configuration. It suggests a significant modification of the channel under the contact. Moreover, it is apparent that for sample #2 2-terminal measurement cannot be obtained by summing up both 3-terminals and 4-terminal measurements. For this sample the leakage current between the Si gate and the germanane flake was found to be relatively high compared to sample #1 and reached up to 3 nA which is comparable to the applied current and, therefore, is likely to influence the measured voltage in all configuration. Leakage current for sample #1 was found to be below the noise level of the measurement (typically $\sim 1 \text{ nA}$) at all gate voltages.

Besides the leakage sample #2 showed a qualitatively similar behaviour to the sample discussed in the main text, including the value for the hole mobility $\sim 400 \text{ cm}^2/(\text{V}\cdot\text{s})$ estimated from 4-terminal measurements at 77 K.

References

- [1] G. Sheldrick, A short history of SHELX, *Acta Crystallographica Section A* 64(1) (2008) 112-122.
- [2] A. Larson, R. Von Dreele, *General Structure Analysis System (GSAS)*; Los Alamos National Laboratory: Los Alamos, NM, 2004; Report LAUR 86-748, There is no corresponding record for this reference.
- [3] E. Bianco, S. Butler, S. Jiang, O.D. Restrepo, W. Windl, J.E. Goldberger, Stability and Exfoliation of Germanane: A Germanium Graphane Analogue, *ACS Nano* 7(5) (2013) 4414-4421.
- [4] X. Luo, E. Zurek, Crystal Structures and Electronic Properties of Single-Layer, Few-Layer, and Multilayer GeH, *The Journal of Physical Chemistry C* 120(1) (2016) 793-800.
- [5] S. Jiang, S. Butler, E. Bianco, O.D. Restrepo, W. Windl, J.E. Goldberger, Improving the stability and optical properties of germanane via one-step covalent methyl-termination, *Nature Commun.* 5 (2014).
- [6] Z. Liu, Z. Lou, Z. Li, G. Wang, Z. Wang, Y. Liu, B. Huang, S. Xia, X. Qin, X. Zhang, Y. Dai, GeH: a novel material as a visible-light driven photocatalyst for hydrogen evolution, *Chemical Communications* 50(75) (2014) 11046-11048.
-